Magnetization reversal via internal spin waves in magnetic nanoparticles

D. A. Garanin[1] and H. Kachkachi[2]
[1]*Department of Physics, Lehman College, City University of New York, 250 Bedford Park Boulevard West, Bronx, New York 10468-1589, USA*
[2]*Laboratoire de Mathématiques, Physique et Systèmes, Université de Perpignan via Domitia, 52 Avenue de Paul Alduy, 66860 Perpignan Cedex, France*

(Received 9 February 2009; revised manuscript received 10 June 2009; published 20 July 2009)

By numerically solving the equations of motion for atomic spins we show that internal spin-wave processes in large enough magnetic particles, initially in unstable states, lead to complete magnetization reversal and thermalization. The particle's magnetization m strongly decreases in the middle of reversal and then recovers. The closer is the initial orientation of $\mathbf{m}$ to the energy minimum, the slower is the relaxation toward it and the smaller is the decrease in m in the course of relaxation. We identify two main scenarios, exponential and linear spin-wave instabilities. For the latter, the longitudinal and transverse relaxation rates have been obtained analytically. Orientation dependence of these rates leads to a nonexponential relaxation of the particle's magnetization at long times.

DOI: 10.1103/PhysRevB.80.014420 PACS number(s): 75.50.Tt, 75.75.+a, 75.30.Ds, 76.20.+q

I. INTRODUCTION

From both fundamental and application viewpoints, the switching time required for the magnetization reversal has become of utmost significance today. The tremendous increase in storage density and read-write speed in magnetic storage media is reaching its limits and the need for further speedup of the magnetization dynamics is one of the main issues. Actual read-write processes operate on the order of nanoseconds and newly developed methods such as precessional switching[1] have demonstrated the possibility to reach subnanosecond time scales. Recent pump-probe experiments have also shown a fast decay of the magneto-optical signal occurring on the subpicosecond time scale using time-resolved techniques such as, to cite a few, the magneto-optical Kerr effect,[2] time-resolved second-harmonic generation,[3] and pulsed inductive microwave magnetometer.[4]

These techniques also make it possible to prepare the system in a nonequilibrium state with the magnetization vector pointing in a freely chosen arbitrary direction. In particular, unlike linear ferromagnetic resonance (FMR) experiments, large-angle motion of the magnetization can be studied. This is relevant to technological applications since magnetic recording heads are expected to change magnetization directions over large angles at ever increasing frequencies. Another advantage of these techniques is that they are sensitive to spin wave and damping phenomena.[5–7]

In this paper we will study the relaxational switching of the magnetization initially put in a state far from equilibrium, as it is possible to do with the methods mentioned above. In general, relaxation is accompanied by a change in the energy of the relaxing system and the energy released or absorbed has to be accommodated by a larger system serving as a heat bath. In particular, magnetization reversal of (quasisingle domain) magnetic particles toward equilibrium reduces their Zeeman and/or anisotropy energy and the role of heat bath can be played by phonons and/or conduction electrons, etc. Most of the existing theories consider magnetic particles as *single macroscopic magnetic moments* whose dynamics is described by the Landau-Lifshitz equation with damping[8] and Langevin noise field (see, e.g., Refs. 9–11) or the corresponding Fokker-Planck equation.

As was pointed out by Suhl[12] and demonstrated by Safonov and Bertram,[13,14] internal spin-wave (SW) modes in the particle can serve as a heat bath and thus be responsible for the particle's relaxation far from equilibrium and thereby for magnetization switching. As a rule, this internal relaxation process should be much faster than those processes that operate via nonmagnetic degrees of freedom with important implications in engineering of magnetic elements in electronics. Progress in computing has made it possible to simulate the dynamics of magnetic particles as systems of *many interacting spins*,[13,14] considered classically. Simulations show that relaxation via internal SW indeed occurs.

From the theoretical viewpoint, SW dynamics in a magnetic particle whose global magnetization strongly depends on time in the course of reversal is a new and challenging subject. Dynamics involving *moderate* deviations in the particle's magnetization from equilibrium, including the Suhl SW instabilities[15] that may lead to a much faster relaxation,[7,12,16] can still be described with the help of a nonlinear SW theory built around the ground state. To the contrast, large deviations require redefinition of the spin-wave vacuum by considering SW dynamics in the frame related to the instantaneous particle's global magnetization. The vacuum corresponding to a collinear state with all particle's spins oriented in an arbitrary direction is an example of a *false vacuum* that is unstable and decays toward the true vacuum. A spin-wave vacuum of this kind was suggested for the thermodynamics of low-dimensional magnetic systems in zero field that have a zero order parameter at $T>0$.[17] Its extension to nonzero field was done in Ref. 18. Recently, the initial stages of SW dynamics including instabilities have been considered in the global-magnetization frame in Ref. 19.

The false-vacuum initial condition can be created by biasing the system with a magnetic field that leads to the disappearance of the metastable energy minimum in which the magnetization is set.[13] Other methods are the precessional[20]

and current-induced[21] switching that allow to rotate the magnetization into an arbitrary direction during the time that is shorter than the relaxation time.

The aim of this paper, which is the extended version of the preceding letter,[22] is twofold: (i) We show by numerical simulations for atomic spins on the lattice at initially $T=0$ that, for particles large enough, excitation of internal spin waves leads to a full magnetization switching and relaxation to a thermal state with the temperature T defined from the energy balance. This solves the puzzle of "incomplete relaxation" observed in Ref. 13 for a particle of only 64 effective spins. We show that magnetization switching via internal spin waves is typically accompanied by a strong reduction in the particle's magnetization m that subsequently recovers to a value that is slightly less than the initial value $m=1$ for collinear spins. This longitudinal relaxation is similar to that described by the Landau-Lifshitz-Bloch (LLB) equation (see, e.g., Refs. 10 and 11), although it has a different origin. (ii) In addition to the *exponential instability* mechanism that occurs in the case of elliptic magnetization precession,[12,13,15,16,19] there occurs a *linear instability* mechanism for the circular magnetization precession. The latter may be driven by a random core (volume) anisotropy or by a surface anisotropy that causes spin noncollinearities. We analytically derive the rates describing the creation of SWs out of the false vacuum, using the spin-wave theory in the frame of the particle's global magnetization $\mathbf{m}$. Essential dependence of these rates on the angle between $\mathbf{m}$ and the magnetic field $\mathbf{H}$, which shapes the energy landscape, leads to a slow nonexponential relaxation of $\mathbf{m}$ at large times.

The remainder of the paper is organized as follows. Section II introduces the classical-spin model of a magnetic particle including a bulk anisotropy and a random anisotropy. Here the existence of two types of SW instabilities is demonstrated. Section III contains the formalism of spin-wave theory in the frame related to particle's global magnetization. The details of the full analytical solution in the case of random anisotropy are given in the Appendix. In Sec. IV the results of numerical atomistic simulations are presented that show the two instability scenarios leading to the magnetization reversal. Section V contains discussion.

II. HAMILTONIAN AND SPIN-WAVE INSTABILITIES

A. Hamiltonian

We consider the classical Hamiltonian ($|\mathbf{s}_i|=1$) on the lattice

$$\mathcal{H}=\sum_i \mathcal{H}_{Ai}-\mathbf{h}\cdot\sum_i \mathbf{s}_i-\frac{1}{2}\sum_{ij} J_{ij}\mathbf{s}_i\cdot\mathbf{s}_j, \tag{1}$$

where $\mathbf{h}=\mu_0\mathbf{H}$, μ_0 is the magnetic moment associated with the spin, $\mathbf{H}$ is the magnetic field, J_{ij} is the exchange interaction, and $\mathcal{H}_{Ai}$ is the crystal-field energy at site i, a function of $\mathbf{s}_i$ satisfying the symmetry of the problem. In applications below, we will consider the bulk uniaxial anisotropy with easy axis $\mathbf{e}_z$

$$\mathcal{H}_{Ai}=-D(\mathbf{e}_z\cdot\mathbf{s}_i)^2,\quad D>0 \tag{2}$$

and the random anisotropy

$$\mathcal{H}_{Ai}=-\sum_{\alpha\beta} g_{i,\alpha\beta}s_{i\alpha}s_{i\beta} \tag{3}$$

with

$$g_{i,\alpha\beta}=D_R\left(u_{i\alpha}u_{i\beta}-\frac{1}{3}\delta_{\alpha\beta}\right),\quad D_R>0 \tag{4}$$

$\mathbf{u}_i$ being a unit vector assuming random directions.[23,24] One can also add a surface anisotropy and dipole-dipole interaction. Throughout the paper we do not include any coupling to the environment.

The particle's magnetization is defined as

$$\mathbf{m}=\frac{1}{\mathcal{N}}\sum_i \mathbf{s}_i, \tag{5}$$

where $\mathcal{N}$ is the total number of spins.

Atomic spins obey the Larmor equation

$$\dot{\mathbf{s}}_i=[\mathbf{s}_i\times\mathbf{\Omega}_i],\quad \hbar\mathbf{\Omega}_i=-\partial\mathcal{H}/\partial\mathbf{s}_i. \tag{6}$$

B. Spin-wave instabilities

We now study two models, one with uniaxial anisotropy with the same easy axis for all spins and no random anisotropy ($D_R=0$), and the other with random anisotropy and no uniaxial anisotropy ($D=0$). We will show that in the case of uniaxial anisotropy the SW instabilities are exponential while in the case of random anisotropy these instabilities are linear. The calculations are both analytical and numerical in the latter case and only numerical in the former.

1. Uniaxial anisotropy and exponential instabilities

The first model we study is that of uniaxial anisotropy with the common easy axis in the z direction, noncollinear with the applied field $\mathbf{h}$. In this case, the spin precession is noncircular. The same effect may also be caused by a *biaxial* anisotropy. We choose the initial state $\mathbf{s}_i=\mathbf{e}_x$ and $\mathbf{h}=h\mathbf{e}_x$. Linearization around this state yields the SW spectrum

$$\varepsilon_{\mathbf{k}}=\sqrt{(h+J_0-J_{\mathbf{k}})(h-2D+J_0-J_{\mathbf{k}})}, \tag{7}$$

where $J_{\mathbf{k}}$ is the Fourier coefficient of J_{ij} which, for a particle with simple-cubic (sc) structure, reads

$$J_{\mathbf{k}}=2J\sum_\alpha \cos(ak_\alpha), \tag{8}$$

where a is the lattice spacing. In the long-wavelength limit $J_0-J_{\mathbf{k}}\cong J(ak)^2$.

Let us now consider the properties of Eq. (7) in different regions of the magnetic field h. (i) For $h>2D$ the state $\mathbf{s}_i=\mathbf{e}_x$ is the energy minimum and thus $\varepsilon_{\mathbf{k}}$ is real. This means that there are no SW instabilities and the initially excited SW will maintain their amplitudes. (ii) In the interval $0<h<2D$ the state $\mathbf{s}_i=\mathbf{e}_x$ is a saddle point, so that $\mathbf{m}$ can rotate away from this state, similarly to the case studied in Ref. 13 (cf. Fig. 1). SW modes in the interval $0<J_0-J_{\mathbf{k}}<2D-h$ are unstable since $\varepsilon_{\mathbf{k}}$ becomes imaginary.[19] This leads to the exponential increase in the

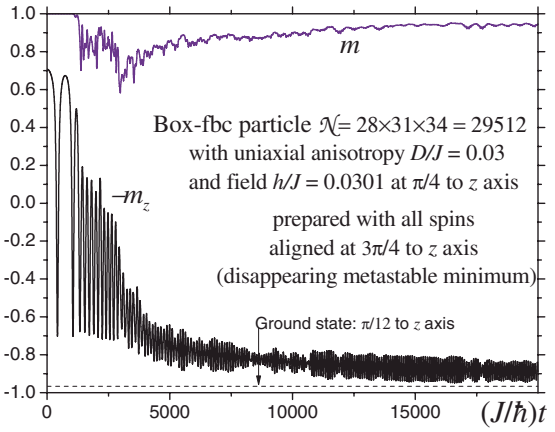

FIG. 1. (Color online) Magnetization switching out of the disappearing metastable state via exponential spin-wave instability in a particle of a box shape with uniaxial anisotropy and oblique magnetic field.

deviations from the initial nearly collinear state. The highest instability increment is realized in the middle of the $\mathbf{k}$ interval of instability, i.e., $J_0-J_{\mathbf{k}}=D-h/2$. This means that exponentially growing spin waves with this nonzero value of $\mathbf{k}$ dominate in the instability process. As a result, the magnetization length $m\equiv|\mathbf{m}|$ decreases upon rotation out of the saddle point, as was observed in early simulations.[13] (iii) For $h<0$ the state $\mathbf{s}_i=\mathbf{e}_x$ is the energy maximum and thus $\mathbf{m}$ performs small-amplitude precession around $\mathbf{e}_x$ in the absence of SW processes. Indeed, according to Eq. (7), the mode $\mathbf{k}=\mathbf{0}$ is stable as $\varepsilon_{\mathbf{0}}$ is real. On the other hand, $\mathbf{k}\neq\mathbf{0}$ modes in the interval

$$-h<J_0-J_{\mathbf{k}}<2D-h \tag{9}$$

are unstable. In this case the only way of reversal is via excitation of internal spin waves with $\mathbf{k}\neq\mathbf{0}$ that strongly reduce the magnetization magnitude m (see Figs. 2 and 3).

2. Random anisotropy and linear instabilities

The second situation we consider here is $D=0$ and nonzero random anisotropy of Eq. (3). The latter does not break the global particle's magnetic isotropy and its only role is to provide strength for SW conversion processes that lead to nonconservation of $\mathbf{m}\cdot\mathbf{h}$ and thus to reversal. We choose $\mathbf{h}=h\mathbf{e}_z$ with $h>0$. Here the precession of $\mathbf{m}$ is circular and there are no exponential SW instabilities. Instead, spin waves may be generated out of a false vacuum by linear transformation processes. In particular, for $\mathbf{m}$ antiparallel to $\mathbf{h}$, spin waves in the particle have a negative gap $-h$. Thus a SW with $\mathbf{k}\neq\mathbf{0}$ can be created out of the false vacuum if its energy is zero:

$$\varepsilon_{\mathbf{k}}=-h+J_0-J_{\mathbf{k}}=0. \tag{10}$$

In Sec. III and the Appendix this process will be considered in detail for any angle between $\mathbf{m}$ and $\mathbf{h}$. The amplitudes of

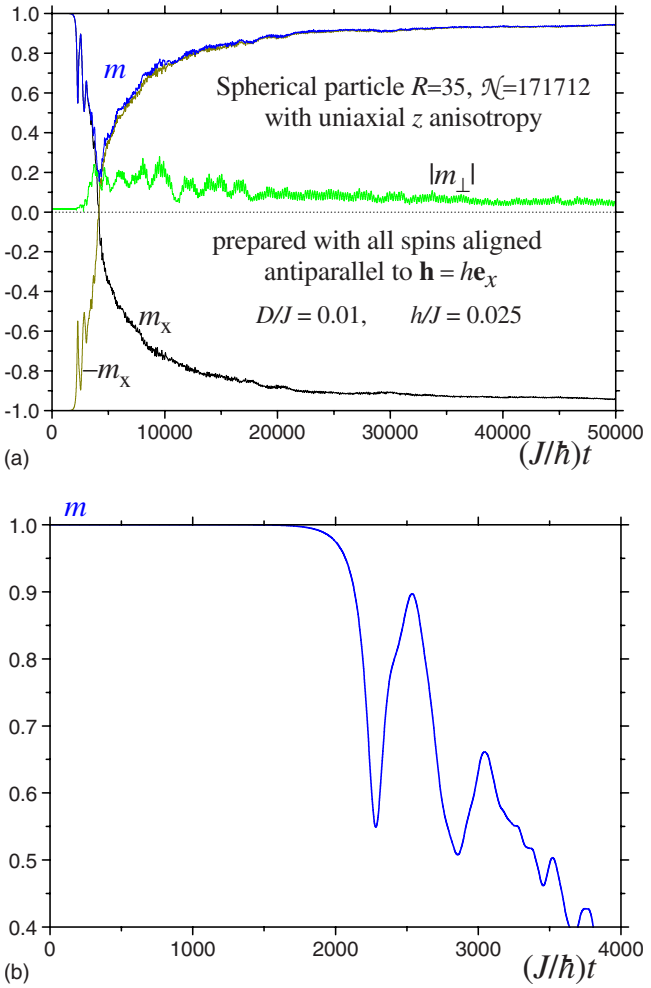

FIG. 2. (Color online) Magnetization switching out of the maximal-energy state via exponential spin-wave instability in a spherical particle with uniaxial anisotropy and transverse field. Switching occurs via longitudinal relaxation without rotation. (b) shows the short-time magnification. The "Plateau" at $t\lesssim 2000$ describes the initial exponential increase in $1-m$.

unstable SW and the deviation of m from saturation increase linearly with time at small times (see Fig. 4).

3. Size effects

In the analysis of both exponential and linear SW instabilities one has to take into account the fact that because of the finite size of magnetic particles their internal SW modes are discrete. In particular, for a box-shaped particle with free boundary conditions (fbc) there are standing spin waves with wave vectors[18]

$$k_\alpha=\frac{\pi n_\alpha}{aN_\alpha},\quad n_\alpha=0,1,\ldots,N_\alpha-1,\quad \alpha=x,y,z, \tag{11}$$

where a is the lattice spacing and $N_xN_yN_z=\mathcal{N}$ is the total number of spins. For most of other shapes, SW modes in magnetic particles have to be found numerically and they are labeled by discrete wave numbers rather than by the wave vector $\mathbf{k}$. In the sequel, in the analytical calculations, we will consider only the box-shaped particles for simplicity.

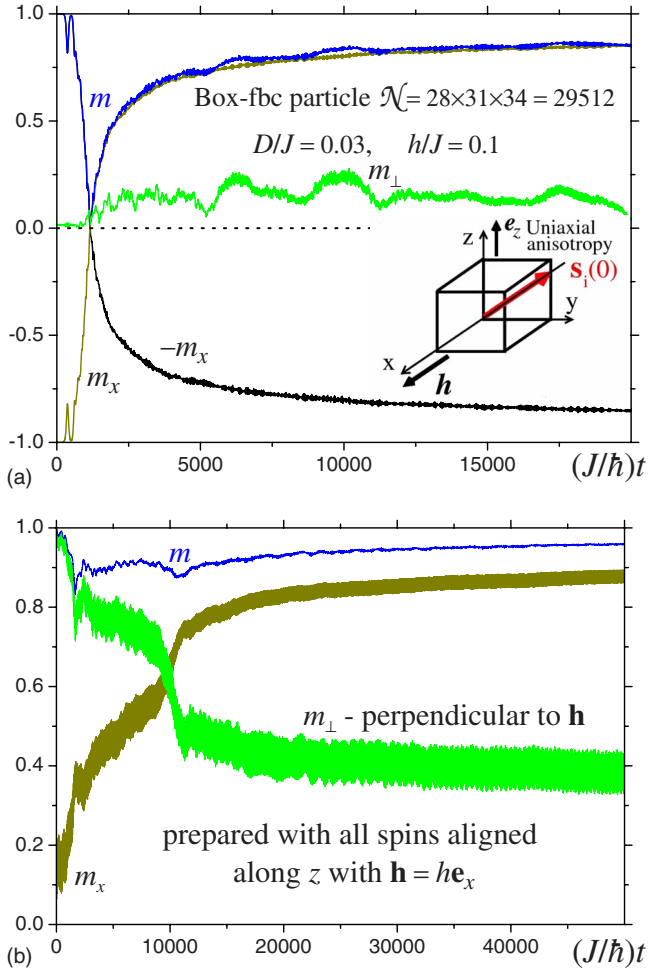

FIG. 3. (Color online) Magnetization switching via exponential spin-wave instability in a box-shaped particle with uniaxial anisotropy and transverse field. (a) The particle is prepared with all spins opposite to the magnetic field (the maximal-energy state). Again the longitudinal relaxation is the main mechanism of switching. (b) The particle is prepared with all spins perpendicular to the magnetic field.

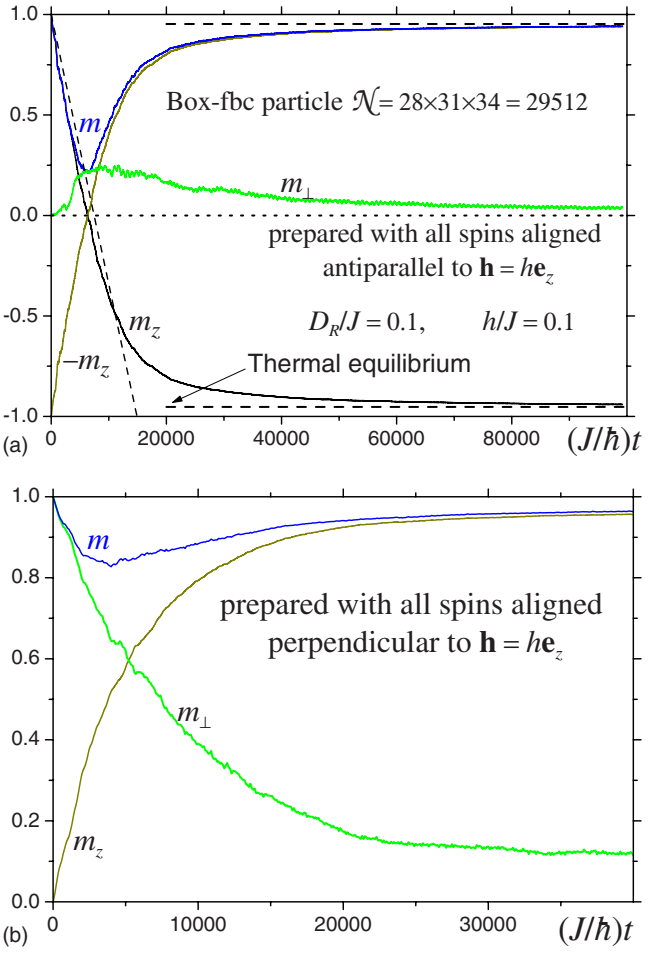

FIG. 4. (Color online) Magnetization switching via linear spin-wave instability in a particle with random anisotropy. (a) Particle prepared with all spins antiparallel to the magnetic field. The small-t asymptote of Eq. (41) is shown by the dashed line. For this initial condition, switching occurs predominantly via changing the magnetization length m. (b) Particle prepared with all spins perpendicular to the magnetic field.

One can see that for the linear instability process, Eq. (10) may be satisfied for a particular SW mode. For particles small enough, the lowest value of $J_0 - J_\mathbf{k}$ for $\mathbf{k} \neq \mathbf{0}$ [i.e., for $n_\alpha = 1$ in Eq. (11)] exceeds h and thus SWs cannot be created. This yields the absolute stability criterion for the particle's linear size L

$$L < L^* = aN^* = \pi a\sqrt{J/h} \tag{12}$$

assuming a cubic shape. If there is only one mode that exactly or approximately satisfies Eq. (10) and this mode does not decay into second-generation SW, there are harmonic oscillations between the false-vacuum state and the state with the resonant SW mode: $1 - m \sim \cos(\Omega t)$, where Ω depends on the strength of the SW conversion processes, i.e., on the random anisotropy or other interactions creating spin noncollinearity. These oscillations are similar to the probability oscillations between two resonant states in quantum mechanics. If the unstable spin-wave mode can be converted into a second-generation spin-wave mode that also has its energy close to zero, the relaxation process becomes at least a two-step process. Conversion into second-generation spin waves already can lead to complete relaxation, as shown by the example in Sec. IV B. For small enough particles, but with $L \gtrsim L^*$, there are not enough resonant SW modes, so that the relaxation process gets stuck in what can be called "spin-wave bottleneck" and the relaxation is incomplete, as was observed in Ref. 13. In large particles, $L \gg L^*$, the spectrum of SW modes become quasicontinuous, the SW bottleneck disappears, and a cascade of SW processes leads to a nearly full magnetization reversal, as is demonstrated below.

Analysis of the exponential instability in magnetic particles of finite size goes along similar lines. The particle is *stable* if the smallest value of $J_0 - J_\mathbf{k}$ with $\mathbf{k} \neq \mathbf{0}$ (i.e., $n_\alpha = 1$) exceeds the right boundary of the instability interval, i.e., $2D - h$, see Eq. (9). This leads to the stability criterion

$$L < L^* = aN^* = \pi a \sqrt{\frac{J}{2D + |h|}} \tag{13}$$

for the particle's size $L=\max(L_x,L_y,L_z)$. Equation (13) is similar to the single-domain criterion since its right-hand side (rhs) is the domain-wall width, if $h=0$. If $L \gtrsim L^*$ and there is only one SW mode inside the instability interval that does not convert into second-generation spin waves, its amplitude and thus the magnetization length m depends periodically on time. This dependence is not sinusoidal, as that for the linear instability, see comment below Eq. (12). Instead, the SW amplitude initially exponentially increases but then this evolution becomes inverted due to nonlinear effects at large amplitudes and the SW amplitude reversibly returns to the starting small value. After that the process repeats periodically. If second-generation unstable spin waves are created, the time evolution of $\mathbf{m}$ becomes more complicated and m does not return to saturation. Still, for $L \gtrsim L^*$ the magnetization reversal is incomplete, as observed in Ref. 13. Only for large enough particles, $L \gg L^*$, does relaxation via internal spin waves lead to a complete magnetization reversal.

Finally, we address the question as to how large the particle must be so that its spectrum of spin waves becomes effectively continuous. In the case of the exponential instability, the criterion is that there must be several modes within the instability interval whose length (in energy) is proportional to D, as we have seen above [see Eq. (9)]. Thus the criterion of the quasicontinuous spectrum becomes

$$\Delta\varepsilon \lesssim D, \tag{14}$$

where $\Delta\varepsilon$ is the average distance between the SW modes. In the case of random anisotropy, the spin-wave deviations, associated with a particular mode, satisfy linear differential equations with a source that is proportional to the random-anisotropy constant D_R, see, e.g., Eq. (A23). The response to the off-resonance source is of order $D_R/\Delta\varepsilon$ that becomes large for $\Delta\varepsilon \lesssim D_R$, formally coinciding with Eq. (14). If this condition is fulfilled, spin waves are effectively generated for all values of the field h without the necessity to satisfy Eq. (10). Next, $\Delta\varepsilon$ can be expressed via the density of SW states, defined by Eq. (A25), as

$$\Delta\varepsilon = \frac{\hbar}{\mathcal{N}\rho(\omega)} \tag{15}$$

in the vicinity of the energy $\varepsilon=\hbar\omega$. Thus Eq. (14) can be rewritten in terms of the particle's size as

$$\mathcal{N} \gtrsim \frac{\hbar}{\rho(\omega)D}. \tag{16}$$

Using $\rho(\omega)$ of Eq. (A27) with $\varepsilon \sim D$ for the model with uniaxial anisotropy, one obtains the criterion of the quasicontinuous spectrum in the form

$$\mathcal{N} \gtrsim (2\pi)^2 (J/D)^{3/2}. \tag{17}$$

For the model with random anisotropy one uses $\varepsilon \sim h$ to obtain the criterion

$$\mathcal{N} \gtrsim (2\pi)^2 (J/D_R)\sqrt{J/h}. \tag{18}$$

For metallic Co one has $D=0.0024J$ so that Eq. (17) yields $\mathcal{N} \gtrsim 336000$.

III. ANALYTICAL THEORY OF SPIN-WAVE INSTABILITIES IN THE PARTICLE FRAME

In this section, we present our general formalism of SW theory in the frame related with the particle's global magnetization for an arbitrary direction of the applied field. Then, we study the two anisotropy models of Secs. II B 1 and II B 2 and the ensuing SW instabilities.

The microscopic effective field $\hbar\boldsymbol{\Omega}_i$ in Eq. (6) can be written in the form

$$\hbar\boldsymbol{\Omega}_i = \mathbf{h} - \frac{\partial \mathcal{H}_{Ai}}{\partial \mathbf{s}_i} + 2\overleftrightarrow{\mathbf{g}}_i \mathbf{s}_i + \sum_j J_{ij}\mathbf{s}_j, \tag{19}$$

where $\mathcal{H}_{Ai}$ contains only nonrandom anisotropy, whereas the random anisotropy is singled out in the third term. In particular, for $\mathcal{H}_{Ai}$ given by Eq. (2) one has $-\partial\mathcal{H}_{Ai}/\partial\mathbf{s}_i = \overleftrightarrow{\mathbf{D}}\mathbf{s}_i \equiv \overleftrightarrow{\mathbf{D}}\cdot\mathbf{s}_i$ and the components of the tensor $\overleftrightarrow{\mathbf{D}}$ read $(\overleftrightarrow{\mathbf{D}})_{\alpha\beta} = D\delta_{\alpha z}\delta_{\beta z}$. Similarly, the components of the random-anisotropy tensor are given by $(\overleftrightarrow{\mathbf{g}}_i)_{\alpha\beta} = g_{i,\alpha\beta}$ and Eq. (4). One can represent $\mathbf{s}_i$ in the form

$$\mathbf{s}_i = \mathbf{m} + \boldsymbol{\psi}_i, \quad \sum_i \boldsymbol{\psi}_i = 0, \tag{20}$$

where $\mathbf{m}$ is the average spin defined by Eq. (5) and $\boldsymbol{\psi}_i$ contains the Fourier components with $\mathbf{k} \neq \mathbf{0}$ and describes spin waves in the particle. Whereas in the standard SW theory $\mathbf{m}$ is a constant corresponding to the ground-state orientation, here it is treated as a time-dependent variable. Since the atomic spins are subject to the chiral constraint $\mathbf{s}_i^2 = 1$, one can use[19] $\mathbf{m} = \mathbf{n}\sqrt{1-\boldsymbol{\psi}_i^2}$ with $\mathbf{n}\cdot\boldsymbol{\psi}_i = 0$, where $\mathbf{n}$ is a unit vector. Although this reduces to two the number of the $\boldsymbol{\psi}_i$ components to deal with, the formalism becomes much more cumbersome. The final results, however, are not affected. Thus we decided not to use the chiral constraint explicitly in our presentation. Of course, properly written equations must satisfy this constraint that can be used to check them.

The equation of motion for $\mathbf{m}$ following from Eq. (6) has the form

$$\hbar\dot{\mathbf{m}} = [\mathbf{m} \times \mathbf{h}_{\text{eff}}] + \mathbf{R}. \tag{21}$$

Here

$$\mathbf{h}_{\text{eff}} \equiv \mathbf{h} - \left.\frac{\partial \mathcal{H}_{Ai}}{\partial \mathbf{s}_i}\right|_{\mathbf{s}_i \Rightarrow \mathbf{m}} \tag{22}$$

is the effective field acting on the particle as a whole and does not contain the random anisotropy and exchange coupling. The term $\mathbf{R}$ couples the dynamics of $\mathbf{m}$ to that of spin waves described by $\boldsymbol{\psi}_i$ and it is responsible for the relaxation of $\mathbf{m}$. Calculation yields

$$\mathbf{R} = \frac{1}{\mathcal{N}} \sum_i [(\mathbf{m} \times 2\vec{\mathbf{g}}_i \boldsymbol{\psi}_i) + \{\boldsymbol{\psi}_i \times [\vec{\mathbf{F}} \boldsymbol{\psi}_i + 2\vec{\mathbf{g}}_i (\mathbf{m} + \boldsymbol{\psi}_i)]\}]. \tag{23}$$

Here $\Sigma_i[\mathbf{m} \times 2\vec{\mathbf{g}}_i \mathbf{m}] = 0$ as an average of the random anisotropy, $\Sigma_{ij} J_{ij} [\boldsymbol{\psi}_i \times \boldsymbol{\psi}_j] = 0$ by symmetry, while some other terms vanish by virtue of Eq. (20). The tensor $\vec{\mathbf{F}}$ is given by

$$(\vec{\mathbf{F}})_{\alpha\beta} = - \left. \frac{\partial^2 \mathcal{H}_{Ai}}{\partial s_{i\alpha} \partial s_{i\beta}} \right|_{\mathbf{s}_i \Rightarrow \mathbf{m}} \tag{24}$$

For $\mathcal{H}_{Ai}$ given by Eq. (2) one has $(\vec{\mathbf{F}})_{\alpha\beta} = 2(\vec{\mathbf{D}})_{\alpha\beta} = 2D\delta_{\alpha z}\delta_{\beta z}$.

In turn, the equation of motion for $\boldsymbol{\psi}_i$ can be obtained as

$$\dot{\boldsymbol{\psi}}_i = \dot{\mathbf{s}}_i - \dot{\mathbf{m}} = [\mathbf{s}_i \times \boldsymbol{\Omega}_i] - \dot{\mathbf{m}}. \tag{25}$$

Working out the various terms yields

$$\hbar \dot{\boldsymbol{\psi}}_i = [\mathbf{m} \times 2\vec{\mathbf{g}}_i \mathbf{m}] + \mathbf{A}_i^{(1)} + \mathbf{A}_i^{(2)}, \tag{26}$$

where $\mathbf{A}_i^{(1)}$ contains terms linear in $\boldsymbol{\psi}_i$ and none in $\vec{\mathbf{g}}_j$, while $\mathbf{A}_i^{(2)}$ contains the terms of order $\boldsymbol{\psi}^2$ and $\boldsymbol{\psi}\mathbf{g}$. In the sequel we will keep only $\mathbf{A}_i^{(1)}$ that is responsible for the generation of spin waves out of a false vacuum, whereas $\mathbf{A}_i^{(2)}$ responsible for nonlinear spin-wave processes will be dropped. One has

$$\mathbf{A}_i^{(1)} = [\boldsymbol{\psi}_i \times (\mathbf{h}_{\text{eff}} + J_0 \mathbf{m})] + \left[\mathbf{m} \times \left(\vec{\mathbf{F}} \boldsymbol{\psi}_i + \sum_j J_{ij} \boldsymbol{\psi}_j \right) \right]. \tag{27}$$

The first term in Eq. (26) that causes noncollinearity of spins, is responsible for the linear SW instability. The same effect is produced by surface anisotropy and dipole-dipole interaction.

In Eq. (21) it is convenient to project the relaxation term $\mathbf{R}$ onto $\mathbf{m}$ and the perpendicular directions. For this we introduce orthogonal unit vectors

$$\mathbf{n} = \frac{\mathbf{m}}{m},$$

$$\mathbf{e}_1 = \frac{[\mathbf{n} \times \mathbf{h}_{\text{eff}}]}{|[\mathbf{n} \times \mathbf{h}_{\text{eff}}]|} = \frac{[\mathbf{n} \times \mathbf{h}_{\text{eff}}]}{h_{\text{eff}} \sqrt{1 - x^2}},$$

$$\mathbf{e}_2 = (\mathbf{n} \times \mathbf{e}_1) = \frac{[\mathbf{n} \times (\mathbf{n} \times \mathbf{h}_{\text{eff}})]}{|(\mathbf{n} \times \mathbf{h}_{\text{eff}})|}, \tag{28}$$

where

$$x \equiv \frac{\mathbf{n} \cdot \mathbf{h}_{\text{eff}}}{h_{\text{eff}}} = \frac{\mathbf{m} \cdot \mathbf{h}_{\text{eff}}}{m h_{\text{eff}}}. \tag{29}$$

$\mathbf{R}$ then has the form

$$\mathbf{R} = R_{\parallel} \mathbf{n} + R_1 \mathbf{e}_1 + R_2 \mathbf{e}_2, \tag{30}$$

where $R_{\parallel}$ describes the longitudinal relaxation of the particle's magnetization (change in the magnetization magnitude) while

$$R_2 \equiv R_{\perp} \tag{31}$$

describes the transverse relaxation (rotational relaxation of the magnetization vector), since $\mathbf{e}_2 \cdot \mathbf{n} = 0$. On the contrary, R_1 does not describe any relaxation. It merely describes a small modification of the particle's precession due to excitation of spin waves, an effect that will be neglected here. Explicitly Eq. (21) can now be rewritten as

$$\hbar \dot{\mathbf{m}} = (\mathbf{m} \times \mathbf{h}_{\text{eff}}) + R_{\parallel} \frac{\mathbf{m}}{m} + R_{\perp} \frac{[\mathbf{m} \times (\mathbf{m} \times \mathbf{h}_{\text{eff}})]}{m |(\mathbf{m} \times \mathbf{h}_{\text{eff}})|}, \tag{32}$$

where

$$R_{\parallel} = \mathbf{n} \cdot \mathbf{R}, \quad R_{\perp} = \mathbf{e}_2 \cdot \mathbf{R}. \tag{33}$$

Equation (32) resembles the Landau-Lifshitz-Bloch equation since it includes both the longitudinal and transverse relaxation terms. Ignoring $\mathbf{A}_i^{(2)}$ in Eq. (26), one can solve the resulting linear equation for $\boldsymbol{\psi}_i$, insert the solution into $\mathbf{R}$, and obtain the relaxation terms in Eq. (32) from Eq. (33). Integrating out $\boldsymbol{\psi}_i$ can be done in the particle's frame defined by Eq. (28). It is understood that Eq. (32) is only valid during the initial stage of the evolution out of the completely or nearly collinear state, $|\mathbf{m}| \cong 1$, when the deviations $\boldsymbol{\psi}_i$ due to spin waves are small and can be considered perturbatively.

A. Linear instabilities

Equation (26) without the contribution $\mathbf{A}_i^{(2)}$ can be solved analytically in the case of a pure random anisotropy, $\mathcal{H}_{Ai} = 0$ since then the time dependence of the frame vectors is a simple precession around the external field $\mathbf{h}$. The details can be found in the Appendix. For $D = 0$ the dependence $\mathbf{m}(t)$ [neglecting $\mathbf{R}$ in Eq. (21)] is a circular precession and thus the calculations simplify and lead to the equation of motion

$$\dot{\mathbf{m}} = \frac{1}{\hbar} (\mathbf{m} \times \mathbf{h}) - m^{3/2} \Gamma_{\parallel}(x) \frac{\mathbf{m}}{m} - m^{3/2} \Gamma_{\perp}(x) \frac{[\mathbf{m} \times (\mathbf{m} \times \mathbf{h})]}{m^2 h}. \tag{34}$$

Here the transverse and longitudinal relaxation rates depend on the orientation of the particle's magnetization vector $x \equiv (\mathbf{m} \cdot \mathbf{h})/(mh)$

$$\Gamma_{\parallel}(x) = \frac{2}{15\pi\hbar} \frac{D_R^2}{J} \sqrt{\frac{h}{J}} \Phi_{\parallel}(x) \equiv \Gamma_{\parallel 0} \Phi_{\parallel}(x), \tag{35}$$

$$\Gamma_{\perp}(x) = \frac{1}{5\pi\hbar} \frac{D_R^2}{J} \sqrt{\frac{h}{J}} \Phi_{\perp}(x) \equiv \Gamma_{\perp 0} \Phi_{\perp}(x) \tag{36}$$

with

$$\Phi_{\parallel}(x) = \frac{(1-x)^2}{4} [(1+2x)^2 + \sqrt{2}(1-x^2)], \tag{37}$$

$$\Phi_{\perp}(x) = \frac{1-x}{6} [(1+2x)^2 + \sqrt{2}(1-x)(2+x)]. \tag{38}$$

The applicability of our method requires $\Gamma_{\perp}, \Gamma_{\parallel} \ll \omega_H = h/\hbar$, i.e., the relaxation of the magnetization (as well as the rate of

SW production) is much slower than the magnetization precession considered as unperturbed in the first approximation above.

We note that Eq. (34) is similar to the LLB equation.[10,11] However, it is valid, in general, only for short times, when the number of excited spin waves is still small and $m \cong 1$, so that neglecting $\mathbf{A}_i^{(2)}$ in Eq. (26) is justified. Correspondingly, m in Eq. (34) may be replaced by 1. Of more consequence, however, is to introduce the magnetization direction $\mathbf{n}$ and write $\mathbf{m}=\mathbf{n}m$. Then Eq. (34) can be split into the following two equations

$$\dot{\mathbf{n}} = \frac{1}{\hbar}(\mathbf{n} \times \mathbf{h}) - \Gamma_\perp(x)\frac{[\mathbf{n} \times (\mathbf{n} \times \mathbf{h})]}{h}, \tag{39}$$

where $x \equiv \mathbf{n} \cdot \mathbf{h}/h$ and

$$\dot{m} = -\Gamma_\parallel(x). \tag{40}$$

The small-t behavior

$$m_z(t) = 1 - \Gamma_\parallel(-1)t \tag{41}$$

follows from Eq. (40) and is shown in Fig. 4(a). It agrees well with the numerical result with a small discrepancy stemming from h/J not being small enough to use the analytical expression for the density of states given by Eq. (A27). Equation (40) does not describe the increase in m after switching and its recovery to $m \cong 1$ that is seen in Fig. 4(a).

A striking feature of our result is that both $\Gamma_\perp(x)$ and $\Gamma_\parallel(x)$ vanish for $\mathbf{m} \| \mathbf{h}$ (i.e., for $x=1$) while they reach their maxima at $x=-1$. Thus, initially fast relaxation slows down when the particle approaches equilibrium, see Fig. 4. Indeed, Eq. (39) can be rewritten as

$$\dot{x} = \Gamma_\perp(x)(1 - x^2). \tag{42}$$

In terms of the angular deviation from equilibrium we have

$$y \equiv 1 - \mathbf{n} \cdot \mathbf{h}/h \equiv 1 - x \ll 1 \tag{43}$$

upon which Eq. (42) simplifies into the equation $\dot{y}=-3\Gamma_{\perp 0}y^2$ whose solution reads

$$y(t) = \frac{y(0)}{1 + 3y(0)\Gamma_{\perp 0}t}. \tag{44}$$

It is seen that the long-time asymptote of this solution does not depend on the initial condition $y(0)$ and is given by $y(t)=1/(3\Gamma_{\perp 0}t)$. The full magnetization vector $\mathbf{m}=\mathbf{n}m$ includes m that follows from Eq. (40). The latter becomes $\dot{m}=-(9/4)\Gamma_{\parallel 0}y^2=-(3/2)\Gamma_{\perp 0}y^2=\dot{y}/2$. This yields

$$1 - m(t) = \frac{1}{2}[y(0) - y(t)]. \tag{45}$$

Thus, we see that the deviation $1-m(t)$ remains finite and small for $t \to \infty$ since $y(t) \to 1/(3\Gamma_{\perp 0}t)$ that is the consequence of the relaxation slowing down as $\mathbf{m}$ approaches equilibrium. The change in $\mathbf{m}$ due to its rotation and due to the change in its magnitude are comparable with each other. In addition, one has to remember that the equation of motion for $\mathbf{m}$ was obtained for the initial stage of relaxation only and, in particular, Eq. (40) does not describe thermalization. Still the evidence provided by these analytical calculations of the nonexponential relaxation via internal spin waves in magnetic particles is quite convincing.

B. Exponential instabilities

In the case of pure bulk anisotropy (no random anisotropy and other interactions causing noncollinearity of spins), Eq. (26) with $\mathbf{A}_i^{(2)} \Rightarrow 0$ is a system of uniform linear equations. In general, $\mathbf{m}$ has a nontrivial quasiperiodic time dependence defined by the bulk anisotropy, magnetic field, and the energy associated with $\mathbf{m}$ that is conserved in the absence of the internal spin waves. Excitation of the latter reduces the energy associated with $\mathbf{m}$ so that the total energy is conserved. Mathematically, spin-wave instabilities in this case are exponential divergences of the solution of a system of linear differential equations with periodic coefficients. A well-known example of such instabilities is parametric resonance. In all cases instability requires elliptic or more complicated precession of $\mathbf{m}$. Simple circular precession around the field $\mathbf{h}$ does not lead to exponential instabilities.

From the physical point of view, exponential SW instabilities are similar to the Suhl exponential instabilities. The difference resides mainly in the mathematical description. The Suhl formalism considers spin waves above the true ground state, so that it cannot be applied in situations of large deviations of $\mathbf{m}$ from the energy minimum. The advantage of the present method is that unstable spin waves are described by a linear differential equation with constant coefficients that can easily be solved.

In contrast, the present method using the frame related to the particle's global magnetization can be used for any deviations of $\mathbf{m}$ from the ground state. The price to pay is to deal with differential equations with time-dependent coefficients that are difficult to solve analytically (see also discussion in Ref. 19). However, if $\mathbf{m}$ is initially oriented toward an energy maximum or a saddle point so that it does not evolve in time in the absence of spin waves, one obtains differential equations for the deviations $\boldsymbol{\psi}_i$ with constant coefficients that can easily be solved showing exponential instabilities. In fact, in this case one can just linearize Eq. (6) near a given direction of $\mathbf{m}$, instead of going through the formalism of this section. Examples are considered below Eq. (7).

IV. NUMERICAL RESULTS

A. Relaxation of the magnetization

Efficient magnetization reversal via the SW instability requires a quasicontinuous SW spectrum, i.e., the existence of many SW modes in the instability interval. For this, a *strong* inequality opposite to Eq. (13) should be fulfilled, i.e., the particle's size and/or the anisotropy D should be large enough. To illustrate the process, we have solved Eq. (6) for magnetization switching using the C++-based package *Magnetic Particle* (© H. Kachkachi & L. Reynaud).

For the model with uniaxial anisotropy with easy axis along z, the calculations have been done for two different particle shapes. One is a sphere of radius $R=35$ lattice spacings, cut inside a $70 \times 70 \times 70$ cube resulting in 171 712

atomic spins. The other particle is a parallelepiped consisting of $28\times31\times34=29\,512$ atomic spins. The idea behind choosing all different (linear) sizes is to avoid degeneracy in the energies of SW modes [see Eq. (11)] and ensure a smoother density of states and thus facilitate SW conversion processes. In both cases the initial state is collinear and a very small surface anisotropy was added to create initial very small deviations from collinearity that later exponentially grow. The lattice structure is simple cubic and boundary conditions are free (fbc). The magnetic field is $\mathbf{h}=h\mathbf{e}_x$, with $h>2D$ that creates the energy maximum in the direction opposite to $\mathbf{h}$. The latter is the initial direction of the magnetization in part of the simulations. As stressed above, a particle whose magnetization is oriented toward the energy maximum cannot just rotate out of this orientation (in the absence of a coupling to the environment) because of the energy conservation.

The results shown in Fig. 2(a) for the spherical particle and in Fig. 4(a) for the box-shaped particle are similar. One can see a nearly full reversal via the *longitudinal* relaxation since the transverse magnetization component $m_\perp$ remains small at all times. In the middle of the switching process, excited spin waves almost completely destroy the magnetization m. Then the first-generation long-wavelength SWs of high amplitude convert via nonlinear processes into all possible spin-wave modes and the system thermalizes. Since the thermodynamics of classical spins is mainly determined by short-wavelength modes of high energy, the energy conservation requires that the amplitudes of these SWs be small. This explains the almost full recovery of m after reversal. The asymptotic disordering $1-m>0$ corresponds to the final temperature T following from the energy balance.

The short-time magnification in Fig. 2(b) shows an exponential increase in $1-m$ due to the SW instability until the first dip, followed by an incomplete recovery of m and its further decrease. The same behavior was observed for other particle shapes.

If the initial particle's magnetization makes an angle with the highest-energy direction, the particle's dynamics is a combination of a noncircular precession of $\mathbf{m}$ and relaxation via SW processes, so that our numerical results show a more complicated behavior. The closer is the initial orientation of $\mathbf{m}$ to the energy minimum, the slower is the relaxation toward it and the smaller is the decrease in m in the course of relaxation. The results for the box-shaped particle with its initial magnetization vector perpendicular to the highest-energy direction are shown in Fig. 3(b). One can see that the transverse relaxation is extremely slow in this case so that a prohibitively long computer time is needed to follow the decay $m_\perp\to0$.

Figure 1 shows the magnetization reversal out of a disappearing metastable state for the model with uniaxial z anisotropy and oblique magnetic field applied at the angle $\psi=\pi/4$ to the z axis. For $h=D$ there is a disappearing metastable minimum for the orientation of the spins at $\theta=3\pi/4$ to the z axis. Indeed, the energy $E(\theta)=-D\cos^2\theta-(h/\sqrt{2})\cos\theta-(h/\sqrt{2})\sin\theta$, following from Eqs. (1) and (2), satisfies $E'(\theta)=E''(\theta)=0$ for $h=D$ and $\theta=3\pi/4$. Also one can check that for $h=D$ one has $E'(\theta)=0$ at $\theta=\pi/12$ that is the energy minimum. Notice that for simulations, a slightly higher value of h has been chosen to let $\mathbf{m}$ precess away from the initial state with $\theta=3\pi/4$. One can see that this precession is strongly noncircular and the particle's global magnetization $\mathbf{m}$ tends to return into the initial state that would comply with the energy conservation law for a single spin. However, due to the excitation of internal spin waves in the particle the energy associated with $\mathbf{m}$ decreases so that the returning to the initial orientation is incomplete. After a couple of cycles many exponentially unstable spin waves get excited and a faster relaxation of $\mathbf{m}$ begins. Asymptotically $\mathbf{m}$ approaches the orientation close to the energy minimum at $\theta=\pi/12$ up to thermal disordering. The reduction in m increases exponentially at small times but does not exceed 40% in the middle of relaxation in this case.

Figure 4 shows the results of our numerical simulations for the magnetization switching in the random-anisotropy model described by Eq. (3). The particle is again parallelepiped with fbc, consisting of $28\times31\times34=29\,512$ atomic spins. One can see again a nearly full reversal which is, in contrast to Fig. 2(b), linear at short times. The simulation results at short times are in a reasonable accord with the analytical result in Eq. (41) that is shown by the dashed line. Also shown in Fig. 4(a) is the asymptotic approach of the thermal state with temperature T corresponding to the released Zeeman energy. Note that the reduction in m in the middle of reversal is much stronger for the anticollinear initial state [Fig. 4(a)] than for the perpendicular initial state [Fig. 4(b)], similarly to the case of the exponential instability.

As discussed in Sec. II, in smaller particles SW modes are essentially discrete and SW conversion processes are blocked by the impossibility to satisfy the energy conservation law. Even if one SW mode is generated as a result of exponential or linear instability, it usually cannot be converted into other modes. This leads to the spin-wave bottleneck in the relaxation process via internal spin waves. As an example we consider the sc-lattice cubic particle with $N_x=N_y=N_z=5$ ($\mathcal{N}=125$) the three degenerate modes (1,0,0), (0,1,0), and (0,0,1) are excited via the linear instability process in the model with random anisotropy for the magnetic fields in the vicinity of $h/J=0.38\,197$, as follows from Eqs. (10), (8), and (11). In Fig. 5 obtained with $D_R/J=0.01$ one can see that at $h/J=0.38\,197$ there is an essential reduction in the initially saturated magnetization, although the relaxation is bottlenecked because second-generation spin waves cannot be created. The evolution of m is not sinusoidal because three degenerate SW modes are excited with different efficiencies, depending on the realization of the random anisotropy, so that each mode has its own conversion frequency Ω, mentioned below Eq. (12). On the contrary, for the off-resonance value $h/J=0.37$ there is no SW mode at resonance with the false vacuum and deviations $1-m$ remain very small.

For larger values of the random-anisotropy constant, the particle's SW spectrum becomes effectively continuous, in accordance with the arguments at the end of Sec. II. In particular, for $D_R/J=0.1$ there is no principal difference between the results for $h/J=0.38\,197$ and $h/J=0.37$, and the magnetization relaxes toward the ground state. However, this relaxation is much slower than in really large particles

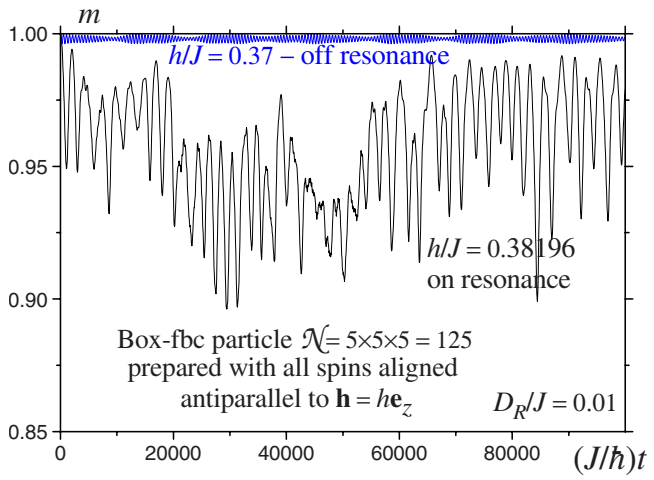

FIG. 5. (Color online) Time dependence of the magnetization magnitude m for a cubic particle of $5\times5\times5=125$ spins with random anisotropy. For the resonant value of the field h spin waves are generated out of the false vacuum (magnetization opposite to the field) but they cannot be converted into other modes so that the process is bottlenecked. For the nonresonant value of h spin waves are practically not generated.

considered above and there is a significant quasirandom dependence of the relaxation rate on model parameters.

B. Evolution of the magnetic structure and Fourier spectrum

As mentioned in Sec. IV A, long-wavelength unstable spin waves of the first generation are converted via nonlinear SW processes into secondary spin waves of shorter wavelengths and the full cascade of such conversion processes finally leads to the equilibrium with a nonzero temperature following from the energy balance. To illustrate this, we calculated magnetic structures and Fourier spectra at different moments of time during relaxation of a box-shaped particle with random uniaxial anisotropy shown in Fig. 6. To save

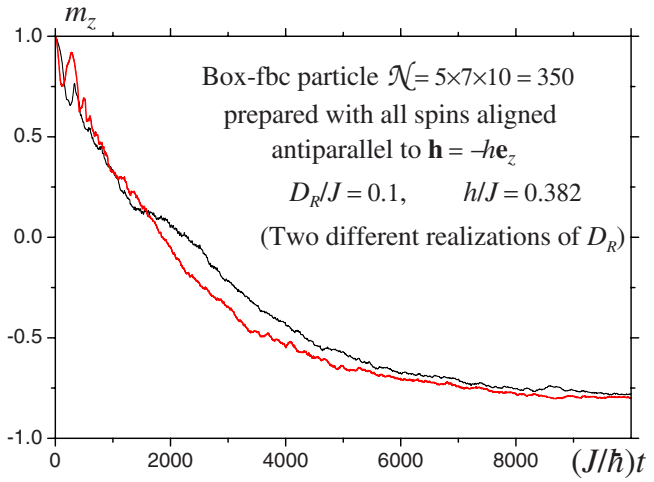

FIG. 6. (Color online) Time dependence of the magnetization component m_z for the box-shaped particle of $5\times7\times10=350$ spins with random anisotropy, initially oriented opposite to the field $h/J=0.382$.

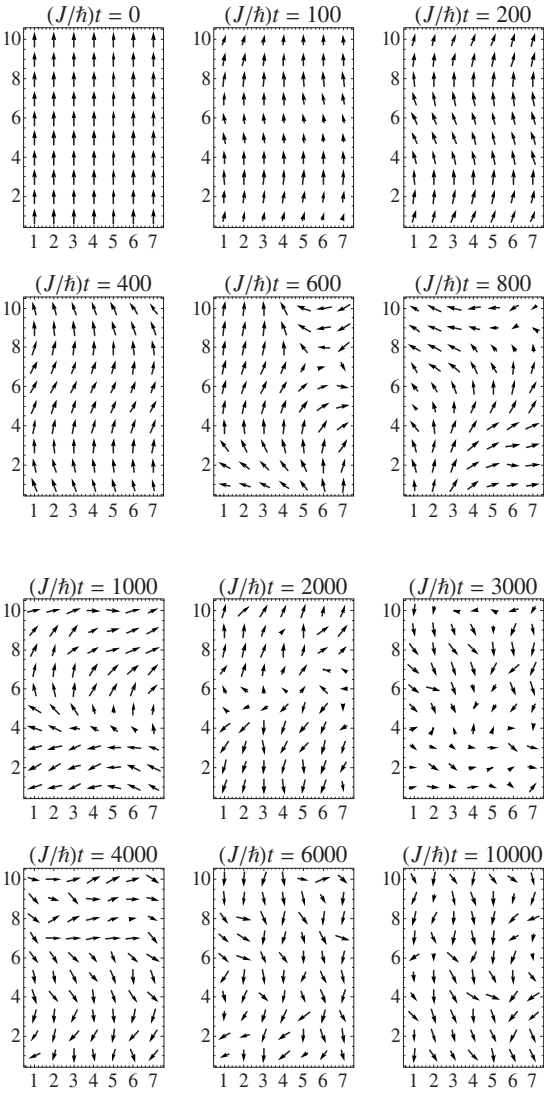

FIG. 7. Spin configurations at different times for the box-shaped particle of $5\times7\times10=350$ with random anisotropy in the middle of the x plane ($i_x=3$).

computer time, we have used a particle of a small size with $\mathcal{N}=5\times7\times10=350$ spins. In the field $h/J=0.382$ the instability condition (10) is satisfied for the modes (1,0,0) and (0,0,2), where we code wave vectors by n_α in Eq. (11). Moreover, there is a second-generation pair of unstable spin waves $(0,0,1)+(1,1,1)$ since $\varepsilon_{0,0,1}+\varepsilon_{1,1,1}=0.0119J$ that is nearly at resonance with $\varepsilon_{1,0,0}=\varepsilon_{0,0,2}\cong0$. As a result, one observes a complete relaxation and thermalization for $D_R/J=0.1$.

For one of the realizations of the random anisotropy, magnetic structures at different moments of time in the middle x plane ($i_x=3$) are shown in Fig. 7. At the initial stage, a high-amplitude long-wavelength excitation is generated. At the end of the evolution, the energy migrates into excitations with higher wave vectors and the magnetic states become thermal.

To describe the evolution of the Fourier spectrum, it is convenient to introduce

$$F_{\mathbf{k}} \equiv \sum_{\alpha} m_{\alpha,\mathbf{k}}^2 \tag{46}$$

as the overall measure of spin fluctuations at a particular $\mathbf{k}$, where

$$\mathbf{m}_{\mathbf{k}} \equiv \frac{1}{\sqrt{\mathcal{N}}} \sum_{i} \mathbf{s}_i f_{i_x,k_x} f_{i_y,k_y} f_{i_z,k_z}, \tag{47}$$

$i \equiv (i_x, i_y, i_z)$, and f_{i_α,k_α} are SW eigenfunctions for a box-shaped crystal with cubic lattice structure and periodic boundary conditions[18]

$$f_{i_\alpha,k_\alpha} = \sqrt{\frac{2}{(1+\delta_{k_\alpha,0})N_\alpha}} \cos[(i_\alpha - 1/2)k_\alpha] \tag{48}$$

and k_α are defined by Eq. (11). The definition of $F_{\mathbf{k}}$ does not depend on the direction of the global magnetization $\mathbf{m}$ of Eq. (5) and this is very convenient in our case. In particular, for the collinear state all Fourier components with $\mathbf{k} \neq \mathbf{0}$ are zero and one obtains $\mathbf{m_0} = \mathbf{m}$ and $F_{\mathbf{0}} = m^2$.

In the course of relaxation in Figs. 2(a), 3(a), and 4(a), as well as Fig. 6 (not shown), the magnetization is nearly destroyed in the intermediate stage and thus $F_{\mathbf{0}}$ drops from 1 to nearly zero and then increases again to nearly 1. To the contrary, $F_{\mathbf{k}}$ with $\mathbf{k} \neq \mathbf{0}$ increase from zero and asymptotically reach nonzero values corresponding to the equilibrium spin waves. $F_{\mathbf{k}}$ with $\mathbf{k}$ corresponding to SW instabilities and around increase to large values as the unstable spin waves are generated but then they decrease to their thermal equilibrium values. $F_{\mathbf{k}}$ with large k always remain small.

The function

$$\bar{E}_{\mathbf{k}} \equiv (J_0 - J_{\mathbf{k}}) F_{\mathbf{k}} \tag{49}$$

describes the distribution of spin-wave energy among different SW modes, the peak at $\mathbf{k}=\mathbf{0}$ being removed. $\bar{E}_{\mathbf{k}}$ is more convenient to represent spin waves over the whole Brillouin zone than $F_{\mathbf{k}}$ since it gives a due weight to excitations with large k that are not seen in $F_{\mathbf{k}}$. When the system reaches equilibrium, $\bar{E}_{\mathbf{k}}$ becomes on average independent of $\mathbf{k}$. It is convenient to represent $\bar{E}_{\mathbf{k}}$ as a function of $J_0 - J_{\mathbf{k}}$, as is done in Fig. 8.

The stages of the evolution of $\bar{E}_{\mathbf{k}}$ shown in Fig. 8 are the following. At short times, Fig. 8(a), the rising peak on the left at $(J_0 - J_{\mathbf{k}})/J \simeq 0.382$ corresponds to the unstable spin waves of the first generation. One can also see a smaller peak to the right of the main peak that corresponds to one of the second-generation SWs. After some time the excitation migrates to other SW modes, the peaks become lower and then disappear completely, and the equilibrium distribution is eventually reached. This thermalization stage is shown in Fig. 8(b).

Let us consider now the thermal equilibrium state at the end of the relaxation. The temperature in the final state can be found from the condition that the Zeeman energy released in the relaxation is converted into thermal energy. For classical systems, as is the case for our model, the energy per degree of freedom is $(1/2)k_BT$. Each SW mode has two degrees of freedom, that is, the total energy in the mode is k_BT.

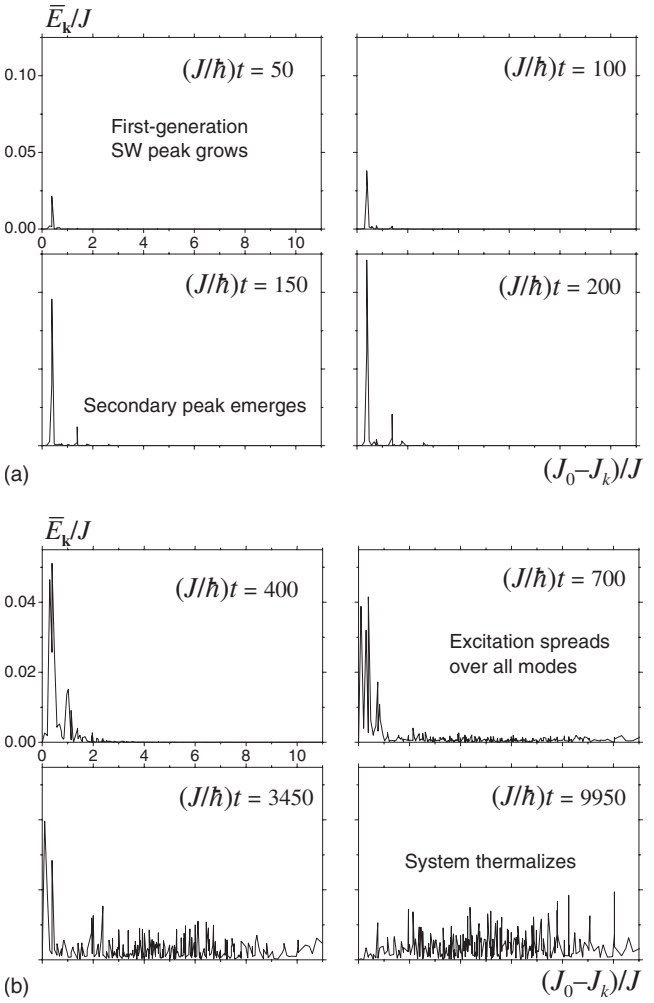

FIG. 8. Fourier spectra at different times for the box-shaped particle of $5\times7\times10=350$ spins with random anisotropy, initially oriented opposite to the field $h/J=0.382$. (a) Initial stage of the instability: growth of the first-generation peak and the secondary peak. (b) Spread of the excitation over all modes and thermalization.

The number if different SW modes are equal to the number of spins in the particle. Thus the energy balance condition per spin/mode has the form

$$k_BT = 2g\mu_BH \equiv 2h \tag{50}$$

since the initial orientation of the spins is opposite to the field whereas the final orientation is parallel to it. At a given temperature $k_BT \ll J_0$, the equilibrium magnetization of a classical-spin system is given by[25]

$$m_{\mathrm{eq}}(T) \cong 1 - \frac{k_BT}{h+J_0} P\left(\frac{J_0}{h+J_0}\right), \tag{51}$$

where $P(z)$ is the so-called lattice Green's function that depends on the lattice structure and is explicitly given by

$$P(z) = \frac{1}{\mathcal{N}} \sum_{n_x=0}^{N_x-1} \sum_{n_y=0}^{N_y-1} \sum_{n_z=0}^{N_z-1} \frac{1}{1 - z\lambda_{\mathbf{k}}}, \tag{52}$$

where $\lambda_{\mathbf{k}} \equiv J_{\mathbf{k}}/J_0$ and $\mathbf{k}$ is given by Eq. (11). For our finite-size system the easiest way is to calculate $P(z)$ by direct summation. For the box particle $28 \times 31 \times 34$ in Fig. 4 in the field $h/J=0.1$ and thus $h/J_0=0.016\,666$ Eq. (52) yields $P(0.9836)=1.48\,286$. Then Eqs. (51) and (50) result in $m_{\mathrm{eq}}=0.97\,569$ that is shown in Fig. 4(a) as thermal equilibrium.

V. DISCUSSION

We have shown that internal spin-wave processes in large enough magnetic particles can lead to complete magnetization reversal and thermalization. The role of thermal bath in these processes is played by the magnetic particle itself. The energy release in the course of the relaxation of the particle's global magnetization **m** toward the ground state is absorbed by internal spin waves so that the total energy is conserved, as long as there is no coupling to the environment.

The two main scenarios of magnetization reversal are through exponential and linear SW instabilities. While the former is the Suhl instability, described here within a more general formalism that allows for large magnetization motions, the linear instability is difficult to pinpoint in the existing literature. Anyway, theoretical description of the linear instability requires redefinition of the spin-wave vacuum by using the frame related to the particle's global magnetization **m** that in general depends on time.

In both cases, the relaxation is fast at the beginning but then slows down. These results are relevant to the study of the dynamics of magnetoelectronic elements and, more generally, in the physics of *unstable* macroscopic states. In the model with random anisotropy that can be solved analytically, relaxation at asymptotically large times is power law rather than exponential. The reason is that the relaxation rate becomes small as the direction of the particle's magnetization approaches the ground-state direction. For the random-anisotropy model both longitudinal and transverse relaxation rates are maximal for **m** pointing toward the energy maximum. It is clear that the majority of the magnetic nanoparticles studied nowadays are shown to exhibit effective uniaxial anisotropy. However, as their size is further reduced, the on-site crystalline anisotropy may adopt a more disordered distribution upon which the model of random anisotropy may become of some relevance.

Estimations of relaxation rates via internal spin waves in metallic Co made in Ref. 22 yield $\Gamma \sim 10^5 - 10^6$ s^{-1}. Comparison with the spin-phonon and other external rates, obtained microscopically, is difficult since the latter are still unreliable and should be modified by collective processes such as phonon bottleneck[26,27] and phonon superradiance.[28] In most cases internal processes should dominate. One should not forget, however, that the latter die out for nanoparticles that cannot accommodate spin waves. The phenomenological Landau-Lifshitz relaxation rate $\Gamma_{LL}=\alpha h/\hbar$ with the damping constant α ranging between 10^{-1} and 10^{-3} is typically much larger than microscopic rates that do not take into account collective processes. One has to be careful, however, since the α that is extracted from experiments may contain a contribution from the SW processes.

Numerical simulations in this work have been done for a classical-spin model without coupling to the environment. The dynamical equations are Larmor equations for each atomic spin precessing in the effective field created by the other spins plus the magnetic and anisotropy fields. Including the effect of the environment by a double vector-product relaxation term introduced by Landau and Lifshitz[8] is straightforward. Furthermore, one can also include the finite-temperature effect through a Langevin field, though with the price that this makes the program much slower. It should be stressed, however, that such a method of including the environment is not fully reliable because it misses collective effects in the spin-lattice relaxation.

ACKNOWLEDGMENTS

D. G. thanks E. M. Chudnovsky for useful discussions. This work has been supported by the Cottrell College Science Award of the Research Corporation. We are greatly indebted to L. Reynaud for his expert support in questions of numerical efficiency.

APPENDIX: RANDOM ANISOTROPY: DYNAMICS IN THE PRECESSING FRAME

Consider a model with $\mathcal{H}_{Ai}=0$ and small random anisotropy $\vec{\mathbf{g}}_i$ that is the only source for the particle's relaxation. In the zeroth approximation **m** is simply precessing around the magnetic field

$$\hbar \dot{\mathbf{m}} = [\mathbf{m} \times \mathbf{h}] \tag{A1}$$

and it is convenient to consider spin waves in the frame related to **m** and defined by Eq. (28). Equations (28) can be solved for **h** resulting in

$$\mathbf{h} = hx\mathbf{n} - h\sqrt{1-x^2}\mathbf{e}_2. \tag{A2}$$

Time derivatives of the basis vectors defined by Eq. (28) are given by [using Eq. (A1)]

$$\hbar \dot{\mathbf{n}} = [\mathbf{n} \times \mathbf{h}],$$

$$\hbar \dot{\mathbf{e}}_1 = \frac{(\hbar \dot{\mathbf{n}} \times \mathbf{h})}{h\sqrt{1-x^2}} = \frac{[(\mathbf{n} \times \mathbf{h}) \times \mathbf{h}]}{h\sqrt{1-x^2}} = \frac{-\mathbf{n}h + \mathbf{h}x}{\sqrt{1-x^2}},$$

$$\hbar \dot{\mathbf{e}}_2 = \frac{\hbar \dot{\mathbf{n}}(\mathbf{n} \cdot \mathbf{h})}{h\sqrt{1-x^2}} = \frac{[\mathbf{n} \times \mathbf{h}]x}{\sqrt{1-x^2}} \tag{A3}$$

and they can be projected on $\mathbf{n}$, $\mathbf{e}_1$, and $\mathbf{e}_2$

$$\hbar \dot{\mathbf{n}} = h\sqrt{1-x^2}\mathbf{e}_1,$$

$$\hbar \dot{\mathbf{e}}_1 = (\mathbf{n} \cdot \hbar \dot{\mathbf{e}}_1)\mathbf{n} + (\mathbf{e}_2 \cdot \hbar \dot{\mathbf{e}}_1)\mathbf{e}_2 = -h\sqrt{1-x^2}\mathbf{n} - hx\mathbf{e}_2,$$

$$\hbar \dot{\mathbf{e}}_2 = hx\mathbf{e}_1. \tag{A4}$$

Now the explicit time dependence has to be obtained. To this end, it is convenient to choose the z axis along $\mathbf{h}$, i.e., $\mathbf{h}=h\mathbf{e}_z$, then from Eq. (A1) follows

$$\mathbf{n}(t) = x\mathbf{e}_z - \sqrt{1-x^2}\cos(\omega_h t)\mathbf{e}_x + \sqrt{1-x^2}\sin(\omega_h t)\mathbf{e}_y,$$

$$\mathbf{e}_1(t) = \cos(\omega_h t)\mathbf{e}_y + \sin(\omega_h t)\mathbf{e}_x,$$

$$\mathbf{e}_2(t) = -\sqrt{1-x^2}\mathbf{e}_z - x\cos(\omega_h t)\mathbf{e}_x + x\sin(\omega_h t)\mathbf{e}_y, \quad \text{(A5)}$$

where

$$\omega_h = h/\hbar. \quad \text{(A6)}$$

One can project $\boldsymbol{\psi}_i$ onto the time dependent $\mathbf{n}$, $\mathbf{e}_1$, and $\mathbf{e}_2$ as

$$\boldsymbol{\psi}_i = \psi_{i0}\mathbf{n} + \psi_{i1}\mathbf{e}_1 + \psi_{i2}\mathbf{e}_2 \quad \text{(A7)}$$

and thus

$$\hbar\dot{\boldsymbol{\psi}}_i = \hbar\dot{\psi}_{i0}\mathbf{n} + \hbar\dot{\psi}_{i1}\mathbf{e}_1 + \hbar\dot{\psi}_{i2}\mathbf{e}_2 + \psi_{i0}\hbar\dot{\mathbf{n}} + \psi_{i1}\hbar\dot{\mathbf{e}}_1 + \psi_{i2}\hbar\dot{\mathbf{e}}_2. \quad \text{(A8)}$$

Inserting this form into Eq. (26) with $\mathcal{H}_{Ai}=0$ and $\mathbf{A}_i^{(2)}$ dropped and projecting onto the three basis vectors one obtains the equation

$$\hbar\dot{\psi}_{i0} - \psi_{i1}h\sqrt{1-x^2} = \mathbf{n}\cdot\mathbf{A}_i^{(1)} \quad \text{(A9)}$$

as well as

$$\hbar\dot{\psi}_{i1} + \psi_{i0}h\sqrt{1-x^2} + hx\psi_{i2} = \mathbf{e}_1\cdot[\mathbf{m}\times 2\vec{\mathbf{g}}_i\mathbf{m}] + \mathbf{e}_1\cdot\mathbf{A}_i^{(1)} \quad \text{(A10)}$$

together with

$$\hbar\dot{\psi}_{i2} - hx\psi_{i1} = \mathbf{e}_2\cdot[\mathbf{m}\times 2\vec{\mathbf{g}}_i\mathbf{m}] + \mathbf{e}_2\cdot\mathbf{A}_i^{(1)}. \quad \text{(A11)}$$

In the rhs of Eq. (A9) one has

$$\mathbf{n}\cdot\mathbf{A}_i^{(1)} = \mathbf{n}\cdot[\boldsymbol{\psi}_i\times\mathbf{h}] = \boldsymbol{\psi}_i\cdot[\mathbf{h}\times\mathbf{n}]. \quad \text{(A12)}$$

Then with the help of the first of Eqs. (28) one obtains

$$\dot{\psi}_{i0} = 0. \quad \text{(A13)}$$

Expressions in the rhs of other equations can be processed as follows

$$\begin{aligned}\mathbf{e}_1\cdot[\mathbf{m}\times\vec{\mathbf{g}}_i\mathbf{m}] &= m^2\mathbf{e}_1\cdot[\mathbf{n}\times\{\mathbf{e}_1(\mathbf{e}_1\vec{\mathbf{g}}_i\mathbf{n}) + \mathbf{e}_2(\mathbf{e}_2\vec{\mathbf{g}}_i\mathbf{n})\}] \\ &= m^2\mathbf{e}_1\cdot\{\mathbf{e}_2(\mathbf{e}_1\vec{\mathbf{g}}_i\mathbf{n}) - \mathbf{e}_1(\mathbf{e}_2\vec{\mathbf{g}}_i\mathbf{n})\} \\ &= -m^2(\mathbf{e}_2\vec{\mathbf{g}}_i\mathbf{n}) \quad \text{(A14)}\end{aligned}$$

and, similarly,

$$\mathbf{e}_2\cdot[\mathbf{m}\times\vec{\mathbf{g}}_i\mathbf{m}] = m^2(\mathbf{e}_1\vec{\mathbf{g}}_i\mathbf{n}). \quad \text{(A15)}$$

From Eq. (27) with $\mathcal{H}_{Ai}=0$ one obtains

$$\begin{aligned}\mathbf{A}_i^{(1)} &= [\boldsymbol{\psi}_i\times(\mathbf{h}+J_0\mathbf{m})] + \left[\mathbf{m}\times\sum_j J_{ij}\boldsymbol{\psi}_j\right] \\ &= [(\psi_{i0}\mathbf{n} + \psi_{i1}\mathbf{e}_1 + \psi_{i2}\mathbf{e}_2)\times(\mathbf{h}+J_0\mathbf{m})] \\ &\quad + \left[\mathbf{m}\times\sum_j J_{ij}(\psi_{j0}\mathbf{n} + \psi_{j1}\mathbf{e}_1 + \psi_{j2}\mathbf{e}_2)\right] \\ &= \psi_{i0}[\mathbf{n}\times\mathbf{h}] + \psi_{i1}([\mathbf{e}_1\times\mathbf{h}] + J_0 m[\mathbf{e}_1\times\mathbf{n}]) \\ &\quad + \psi_{i2}([\mathbf{e}_2\times\mathbf{h}] + J_0 m[\mathbf{e}_2\times\mathbf{n}]) \\ &\quad + m\sum_j J_{ij}(\psi_{j1}[\mathbf{n}\times\mathbf{e}_1] + \psi_{j2}[\mathbf{n}\times\mathbf{e}_2]). \quad \text{(A16)}\end{aligned}$$

With the help of Eqs. (28) and (A2) this becomes

$$\begin{aligned}\mathbf{A}_i^{(1)} &= \psi_{i0}h\sqrt{1-x^2}\mathbf{e}_1 + \psi_{i1}(-hx\mathbf{e}_2 - h\sqrt{1-x^2}\mathbf{n} - J_0 m\mathbf{e}_2) \\ &\quad + \psi_{i2}(hx\mathbf{e}_1 + J_0 m\mathbf{e}_1) + m\sum_j J_{ij}(\psi_{j1}\mathbf{e}_2 - \psi_{j2}\mathbf{e}_1). \quad \text{(A17)}\end{aligned}$$

The components of this vector are

$$A_{i1}^{(1)} = hx\psi_{i2} + m\sum_j (J_0\delta_{ij} - J_{ij})\psi_{j2} + h\sqrt{1-x^2}\psi_{i0},$$

$$A_{i2}^{(1)} = -hx\psi_{i1} - m\sum_j (J_0\delta_{ij} - J_{ij})\psi_{j1}. \quad \text{(A18)}$$

Now Eqs. (A10) and (A11) after simplification become

$$\hbar\dot{\psi}_{i1} = m\sum_j (J_0\delta_{ij} - J_{ij})\psi_{j2} - 2m^2(\mathbf{e}_2\vec{\mathbf{g}}_i\mathbf{n}),$$

$$\hbar\dot{\psi}_{i2} = -m\sum_j (J_0\delta_{ij} - J_{ij})\psi_{j1} + 2m^2(\mathbf{e}_1\vec{\mathbf{g}}_i\mathbf{n}).$$

This is the system of equations describing the generation of internal spin waves in a magnetic particle.

It is convenient to introduce the variables

$$\psi_{i,\pm} = \psi_{i1} \pm i\psi_{i2}, \quad \mathbf{e}_\pm \equiv \mathbf{e}_1 \pm i\mathbf{e}_2 \quad \text{(A19)}$$

so that

$$\mathbf{e}_1 = \frac{1}{2}(\mathbf{e}_- + \mathbf{e}_+), \quad \mathbf{e}_2 = \frac{i}{2}(\mathbf{e}_- - \mathbf{e}_+),$$

$$\psi_{i1} = \frac{1}{2}(\psi_{i,-} + \psi_{i,+}), \quad \psi_{i2} = \frac{i}{2}(\psi_{i,-} - \psi_{i,+})$$

and

$$\begin{aligned}\mathbf{e}_1\psi_{i1} + \mathbf{e}_2\psi_{i2} &= \mathrm{Re}(\mathbf{e}_-\psi_{i,+}), \\ \mathbf{e}_1\psi_{i2} - \mathbf{e}_2\psi_{i1} &= \mathrm{Im}(\mathbf{e}_-\psi_{i,+}), \\ \mathbf{e}_1\psi_{i2} + \mathbf{e}_2\psi_{i1} &= \mathrm{Im}(\mathbf{e}_+\psi_{i,+}). \quad \text{(A20)}\end{aligned}$$

Then one obtains the equation

$$\hbar\dot{\psi}_{i,+} = -im\sum_j (J_0\delta_{ij} - J_{ij})\psi_{j,+} + 2im^2(\mathbf{e}_+\vec{\mathbf{g}}_i\mathbf{n}) \quad \text{(A21)}$$

and the conjugate equation for $\dot{\psi}_{i,-}$.

For a box-shaped particle one can rewrite this equation in terms of the discrete Fourier components

$$\boldsymbol{\psi}_{\mathbf{k}} = \sum_i e^{i\mathbf{k}\cdot r_i}\boldsymbol{\psi}_i, \quad \boldsymbol{\psi}_i = \frac{1}{\mathcal{N}}\sum_{\mathbf{k}} e^{-i\mathbf{k}\cdot\mathbf{r}_i}\boldsymbol{\psi}_{\mathbf{k}}, \tag{A22}$$

etc., as

$$\hbar\dot{\psi}_{\mathbf{k},+} = -i\varepsilon_{\mathrm{ex},\mathbf{k}}\psi_{\mathbf{k},+} + 2im^2(\mathbf{e}_+\vec{\mathbf{g}}_{\mathbf{k}}\mathbf{n}), \tag{A23}$$

where

$$\varepsilon_{\mathrm{ex},\mathbf{k}} = m(J_0 - J_{\mathbf{k}}). \tag{A24}$$

The density of pure-exchange spin-wave states is given by

$$\rho_{\mathrm{ex}}(\omega) = \frac{1}{\mathcal{N}}\sum_{\mathbf{k}} \delta(\omega_{\mathrm{ex},\mathbf{k}} - \omega), \tag{A25}$$

where $\hbar\omega_{\mathrm{ex},\mathbf{k}} = \varepsilon_{\mathrm{ex},\mathbf{k}}$ and $\mathcal{N} = N_x N_y N_z$. It satisfies $\int d\omega\rho(\omega) = 1$. In the continuous approximation for small wave vectors for the sc lattice one has

$$\varepsilon_{\mathrm{ex},\mathbf{k}} \cong mJ(ak)^2. \tag{A26}$$

For a particle of a box shape with fbc for $\hbar\omega \ll J_0$ one obtains

$$\begin{aligned}\rho_{\mathrm{ex}}(\omega) &\cong a^3\int\int\int_0^\infty \frac{dk_x dk_y dk_z}{\pi^3}\delta(\omega_{\mathrm{ex},\mathbf{k}} - \omega)\\ &= \hbar\frac{4\pi a^3}{8\pi^3}\int_0^\infty k^2 dk\,\delta(\varepsilon_{\mathrm{ex},\mathbf{k}} - \varepsilon)\\ &= \frac{\hbar}{(2\pi)^2}\sqrt{\frac{\varepsilon}{m^3 J^3}}.\end{aligned} \tag{A27}$$

Equation (A23) has the solution

$$\begin{aligned}\psi_{\mathbf{k},+}(t) = \psi_{\mathbf{k},+}(0)e^{-i\omega_{\mathrm{ex},\mathbf{k}}t} + 2m^2\frac{i}{\hbar}\int_0^t dt' \times e^{-i\omega_{\mathrm{ex},\mathbf{k}}(t-t')}\\ \times[\mathbf{e}_+(t')\vec{\mathbf{g}}_{\mathbf{k}}\mathbf{n}(t')],\end{aligned} \tag{A28}$$

where $\hbar\omega_{\mathrm{ex},\mathbf{k}} = \varepsilon_{\mathrm{ex},\mathbf{k}}$. The first term of the solution takes into account spin waves already available in the particle, such as thermal spin waves. The second term describes spin waves generated by the particle's precession via the random anisotropy. Note that, according to Eq. (A13), longitudinal fluctuations ψ_{i0} do not have any dynamics in the linear approximation.

The next step is to substitute the solution for $\psi_{\mathbf{k},+}(t)$ into the relaxation term $\mathbf{R}$ in the equation for $\mathbf{m}$, see Eq. (21). Keeping terms of order $\boldsymbol{\psi}\mathbf{g}$ in Eq. (23) with $\mathcal{H}_{Ai} = 0$ one obtains

$$\mathbf{R} = 2m\frac{1}{\mathcal{N}}\sum_i \{[\mathbf{n}\times\vec{\mathbf{g}}_i\boldsymbol{\psi}_i] + [\boldsymbol{\psi}_i\times\vec{\mathbf{g}}_i\mathbf{n}]\}. \tag{A29}$$

For $R_\parallel$ of Eq. (33), using transformations in Eq. (A14) one obtains

$$\begin{aligned}R_\parallel &= 2m\frac{1}{\mathcal{N}}\sum_i \mathbf{n}\cdot(\boldsymbol{\psi}_i\times\vec{\mathbf{g}}_i\mathbf{n})\\ &= -2m\frac{1}{\mathcal{N}}\sum_i \boldsymbol{\psi}_i\cdot(\mathbf{n}\times\vec{\mathbf{g}}_i\mathbf{n})\\ &= -2m\frac{1}{\mathcal{N}}\sum_i \boldsymbol{\psi}_i\cdot\{\mathbf{n}\times[\mathbf{e}_1(\mathbf{e}_1\vec{\mathbf{g}}_i\mathbf{n}) + \mathbf{e}_2(\mathbf{e}_2\vec{\mathbf{g}}_i\mathbf{n})]\}\\ &= -2m\frac{1}{\mathcal{N}}\sum_i \boldsymbol{\psi}_i\cdot[\mathbf{e}_2(\mathbf{e}_1\vec{\mathbf{g}}_i\mathbf{n}) - \mathbf{e}_1(\mathbf{e}_2\vec{\mathbf{g}}_i\mathbf{n})]\\ &= 2m\frac{1}{\mathcal{N}}\sum_i [(\mathbf{e}_2\vec{\mathbf{g}}_i\mathbf{n})\psi_{i1} - (\mathbf{e}_1\vec{\mathbf{g}}_i\mathbf{n})\psi_{i2}].\end{aligned} \tag{A30}$$

Finally, with the help of Eq. (A20)

$$R_\parallel = -2m\ \mathrm{Im}\left[\frac{1}{\mathcal{N}}\sum_i (\mathbf{e}_-\vec{\mathbf{g}}_i\mathbf{n})\psi_{i,+}\right]. \tag{A31}$$

Further one obtains

$$\begin{aligned}R_2 &= \mathbf{e}_2\cdot\mathbf{R}\\ &= 2m\frac{1}{\mathcal{N}}\sum_i \mathbf{e}_2\cdot[(\mathbf{n}\times\vec{\mathbf{g}}_i\boldsymbol{\psi}_i) + (\boldsymbol{\psi}_i\times\vec{\mathbf{g}}_i\mathbf{n})]\\ &= 2m\frac{1}{\mathcal{N}}\sum_i [(\mathbf{e}_1\vec{\mathbf{g}}_i\boldsymbol{\psi}_i) - \boldsymbol{\psi}_i\cdot(\mathbf{e}_2\times\vec{\mathbf{g}}_i\mathbf{n})]\\ &= 2m\frac{1}{\mathcal{N}}\sum_i \{(\mathbf{e}_1\vec{\mathbf{g}}_i\boldsymbol{\psi}_i) - \boldsymbol{\psi}_i\cdot[\mathbf{e}_1(\mathbf{n}\vec{\mathbf{g}}_i\mathbf{n}) - \mathbf{n}(\mathbf{e}_1\vec{\mathbf{g}}_i\mathbf{n})]\}\\ &= 2m\frac{1}{\mathcal{N}}\sum_i [(\mathbf{e}_2\vec{\mathbf{g}}_i\mathbf{e}_1)\psi_{i1} + (\mathbf{e}_2\vec{\mathbf{g}}_i\mathbf{e}_2)\psi_{i2} - \psi_{i1}(\mathbf{n}\vec{\mathbf{g}}_i\mathbf{n})],\end{aligned} \tag{A32}$$

where we have dropped all the terms with ψ_{i0} since they are frozen in and disappear after the averaging over the random anisotropy. This can be rewritten as

$$R_2 = 2m\ \mathrm{Re}\left\{\frac{1}{\mathcal{N}}\sum_i [(\mathbf{e}_1\vec{\mathbf{g}}_i\mathbf{e}_-) - (\mathbf{n}\vec{\mathbf{g}}_i\mathbf{n})]\boldsymbol{\psi}_{i,+}\right\}. \tag{A33}$$

In the Fourier representation $R_\parallel$ and $R_2 \equiv R_\perp$ are given by

$$\begin{aligned}R_\parallel &= -2m\ \mathrm{Im}\left[\frac{1}{\mathcal{N}^2}\sum_{\mathbf{k}} (\mathbf{e}_-\vec{\mathbf{g}}_{-\mathbf{k}}\mathbf{n})\psi_{\mathbf{k},+}\right],\\ R_\perp &= 2m\ \mathrm{Re}\left[\frac{1}{\mathcal{N}^2}\sum_{\mathbf{k}} \times\{(\mathbf{e}_1\vec{\mathbf{g}}_{-\mathbf{k}}\mathbf{e}_-) - (\mathbf{n}\vec{\mathbf{g}}_{-\mathbf{k}}\mathbf{n})\}\psi_{\mathbf{k},+}\right].\end{aligned} \tag{A34}$$

Note the relations

$$\overleftrightarrow{\mathbf{g}}^{*}_{\mathbf{k}} = \overleftrightarrow{\mathbf{g}}_{-\mathbf{k}}, \quad \psi^{*}_{\mathbf{k},\pm} = \psi_{-\mathbf{k},\mp}. \tag{A35}$$

Using Eq. (A28) yields

$$R_{\parallel} = -2m^3\,\mathrm{Re}\left\{\frac{1}{\mathcal{N}^2}\sum_{\mathbf{k}}\frac{1}{\hbar}\int_0^t dt' e^{-i\omega_{\mathrm{ex},\mathbf{k}}(t-t')} \times[\mathbf{e}_-(t)\overleftrightarrow{\mathbf{g}}_{-\mathbf{k}}\mathbf{n}(t)][\mathbf{e}_+(t')\overleftrightarrow{\mathbf{g}}_{\mathbf{k}}\mathbf{n}(t')]\right\}. \tag{A36}$$

Random anisotropy has the form of Eq. (4), so that

$$g_{\mathbf{k},\alpha\beta} = D_R\sum_i e^{i\mathbf{k}\cdot\mathbf{r}_i}u_{i\alpha}u_{i\beta}. \tag{A37}$$

Using the formula for the ensemble averaging on a lattice site i

$$\left\langle\left(u_\alpha u_\beta - \frac{1}{3}\delta_{\alpha\beta}\right)\left(u_\gamma u_\delta - \frac{1}{3}\delta_{\gamma\delta}\right)\right\rangle = \langle u_\alpha u_\beta u_\gamma u_\delta\rangle + \frac{1}{9}\delta_{\alpha\beta}\delta_{\gamma\delta} + (\delta_{\alpha\beta}\delta_{\gamma\delta}+\delta_{\alpha\gamma}\delta_{\beta\delta}+\delta_{\alpha\delta}\delta_{\beta\gamma})(1-\delta_{\alpha\beta\gamma\delta})\frac{1}{15} + \delta_{\alpha\beta\gamma\delta}\frac{1}{5} + \frac{1}{9}\delta_{\alpha\beta}\delta_{\gamma\delta} = \frac{1}{15}(\delta_{\alpha\beta}\delta_{\gamma\delta}+\delta_{\alpha\gamma}\delta_{\beta\delta}+\delta_{\alpha\delta}\delta_{\beta\gamma}) + \frac{1}{9}\delta_{\alpha\beta}\delta_{\gamma\delta}, \tag{A38}$$

whereas the correlator of two g on different lattice sites is zero, one obtains the important formula

$$\frac{1}{\mathcal{N}}\langle(\mathbf{a}\overleftrightarrow{\mathbf{g}}_{\mathbf{k}}\mathbf{b})(\mathbf{c}\overleftrightarrow{\mathbf{g}}_{-\mathbf{k}}\mathbf{d})\rangle = \frac{D_R^2}{15}\{(\mathbf{a}\cdot\mathbf{b})(\mathbf{c}\cdot\mathbf{d})+(\mathbf{a}\cdot\mathbf{c})(\mathbf{b}\cdot\mathbf{d})+(\mathbf{a}\cdot\mathbf{d})(\mathbf{b}\cdot\mathbf{c})\} + \frac{D_R^2}{9}(\mathbf{a}\cdot\mathbf{b})(\mathbf{c}\cdot\mathbf{d}). \tag{A39}$$

In fact, the terms with $(\mathbf{a}\cdot\mathbf{b})(\mathbf{c}\cdot\mathbf{d})$ vanish in the expressions below. With the help of Eq. (A39) one obtains

$$R_{\parallel} = -4m^3\frac{D_R^2}{15}\mathrm{Re}\left[\frac{1}{\mathcal{N}}\sum_{\mathbf{k}}\frac{1}{\hbar}\int_0^t dt' e^{-i\omega_{\mathrm{ex},\mathbf{k}}(t-t')} \times\{[\mathbf{e}_-(t)\cdot\mathbf{e}_+(t')] \times[\mathbf{n}(t)\cdot\mathbf{n}(t')] + [\mathbf{n}(t)\cdot\mathbf{e}_+(t')][\mathbf{e}_-(t)\cdot\mathbf{n}(t')]\}\right]. \tag{A40}$$

After computer algebra using Eqs. (A5) and (A19) one obtains

$$[\mathbf{e}_-(t)\cdot\mathbf{e}_+(t')][\mathbf{n}(t)\cdot\mathbf{n}(t')] + [\mathbf{n}(t)\cdot\mathbf{e}_+(t')][\mathbf{e}_-(t)\cdot\mathbf{n}(t')] = 3x^2(1-x^2) + \frac{1}{2}(1-x)^2(1+2x)^2e^{i\omega_h(t-t')} + \frac{1}{2}(1+x)^2(1-2x)^2e^{-i\omega_h(t-t')} + \frac{1}{2}(1-x)^2(1-x^2)e^{2i\omega_h(t-t')} + \frac{1}{2}(1+x)^2(1-x^2)e^{-2i\omega_h(t-t')}, \tag{A41}$$

where x is given by Eq. (29) and ω_h by Eq. (A6). Since in Eq. (A40) $\omega_{\mathrm{ex},\mathbf{k}}>0$, here one should keep only the resonant terms with $e^{i\omega_h(t-t')}$ and $e^{2i\omega_h(t-t')}$ that satisfy the energy conservation and cause transitions. One obtains

$$R_{\parallel} = -\frac{4m^3D_R^2}{15\hbar}\frac{1}{\mathcal{N}}\sum_{\mathbf{k}}\left\{\frac{1}{2}(1-x)^2(1+2x)^2\pi\delta(\omega_{\mathrm{ex},\mathbf{k}}-\omega_h) + \frac{1}{2}(1-x)^2(1-x^2)\pi\delta(\omega_{\mathrm{ex},\mathbf{k}}-2\omega_h)\right\} = -\frac{2m^3D_R^2}{15\hbar}(1-x)^2[(1+2x)^2\pi\rho_{\mathrm{ex}}(\omega_h) + (1-x^2)\pi\rho_{\mathrm{ex}}(2\omega_h)]. \tag{A42}$$

With the help of Eq. (A27) one obtains

$$R_{\parallel} = -\frac{2m^{3/2}}{15\pi}\frac{D_R^2}{J}\sqrt{\frac{h}{J}}\Phi_{\parallel}(x), \tag{A43}$$

where $\Phi_{\parallel}(x)$ is given by Eq. (37).

For R_2 from Eqs. (A34) and (A28) one obtains

$$R_{\perp} = 4m^3\,\mathrm{Re}\left[\frac{1}{\mathcal{N}^2}\sum_{\mathbf{k}}\frac{i}{\hbar}\int_0^t dt' e^{-i\omega_{\mathrm{ex},\mathbf{k}}(t-t')} \times\{[\mathbf{e}_1(t)\overleftrightarrow{\mathbf{g}}_{-\mathbf{k}}\mathbf{e}_-(t)]-[\mathbf{n}(t)\overleftrightarrow{\mathbf{g}}_{-\mathbf{k}}\mathbf{n}(t)]\}\times[\mathbf{e}_+(t')\overleftrightarrow{\mathbf{g}}_{\mathbf{k}}\mathbf{n}(t')]\right] = \frac{4m^3D_R^2}{15}\mathrm{Re}\left[\frac{1}{\mathcal{N}}\sum_{\mathbf{k}}\frac{i}{\hbar}\int_0^t dt' e^{-i\omega_{\mathrm{ex},\mathbf{k}}(t-t')}\times\{[\mathbf{e}_1(t)\cdot\mathbf{e}_+(t')] \times[\mathbf{e}_-(t)\cdot\mathbf{n}(t')]+[\mathbf{e}_1(t)\cdot\mathbf{n}(t')][\mathbf{e}_-(t)\cdot\mathbf{e}_+(t')] - 2[\mathbf{n}(t)\cdot\mathbf{e}_+(t')][\mathbf{n}(t)\cdot\mathbf{n}(t')]\}\right]. \tag{A44}$$

Computer algebra yields

$$\frac{i}{\sqrt{1-x^2}}\{[\mathbf{e}_1(t)\cdot\mathbf{e}_+(t')][\mathbf{e}_-(t)\cdot\mathbf{n}(t')]+[\mathbf{e}_1(t)\cdot\mathbf{n}(t')]\times[\mathbf{e}_-(t)\cdot\mathbf{e}_+(t')]-2[\mathbf{n}(t)\cdot\mathbf{e}_+(t')][\mathbf{n}(t)\cdot\mathbf{n}(t')]\}]$$
$$=-3x^3-\frac{1}{2}(1-x)(1+2x)^2e^{i\omega_h(t-t')}+\frac{1}{2}(1+x)(1-2x)^2e^{-i\omega_h(t-t')}-\frac{1}{2}(1-x)^2(2+x)e^{2i\omega_h(t-t')}+\frac{1}{2}(1+x)^2(2-x)e^{-2i\omega_h(t-t')}. \quad \text{(A45)}$$

This results in

$$R_\perp=-\frac{2m^3D_R^2}{15\hbar}\sqrt{1-x^2}(1-x)\pi\{(1+2x)^2\rho_{\mathrm{ex}}(\omega_h)\times(1-x)(2+x)\rho_{\mathrm{ex}}(2\omega_h)\}. \quad \text{(A46)}$$

Finally, using Eq. (A27) again, this expression can be brought into the form

$$R_\perp=-\frac{m^{3/2}}{5\pi}\frac{D_R^2}{J}\sqrt{\frac{h}{J}}\sqrt{1-x^2}\Phi_\perp(x), \quad \text{(A47)}$$

where $\Phi_\perp(x)$ is given by Eq. (38). Finally, with

$$\Gamma_\parallel(x)=-\frac{1}{\hbar}R_\parallel(x),\quad \Gamma_\perp(x)=-\frac{1}{\hbar}\frac{R_\perp(x)}{\sqrt{1-x^2}} \quad \text{(A48)}$$

one obtains Eq. (34).

[1] Y. Acremann, C. H. Back, M. Buess, O. Portmann, A. Vaterlaus, D. Pescia, and H. Melchior, Science **290**, 492 (2000).
[2] E. Beaurepaire, J.-C. Merle, A. Daunois, and J.-Y. Bigot, Phys. Rev. Lett. **76**, 4250 (1996).
[3] J. Hohlfeld, E. Matthias, R. Knorren, and K. H. Bennemann, Phys. Rev. Lett. **78**, 4861 (1997).
[4] M. L. Schneider, Th. Gerrits, A. B. Kos, and T. J. Silva, Appl. Phys. Lett. **87**, 072509 (2005).
[5] M. van Kampen, C. Jozsa, J. T. Kohlhepp, P. LeClair, L. Lagae, W. J. M. de Jonge, and B. Koopmans, Phys. Rev. Lett. **88**, 227201 (2002).
[6] B. Koopmans, J. J. M. Ruigrok, F. Dalla Longa, and W. J. M. de Jonge, Phys. Rev. Lett. **95**, 267207 (2005).
[7] G. de Loubens, V. V. Naletov, and O. Klein, Phys. Rev. B **71**, 180411(R) (2005).
[8] L. D. Landau and E. M. Lifshitz, Phys. Z. Sowjetunion **8**, 153 (1935).
[9] W. F. Brown, Phys. Rev. **130**, 1677 (1963).
[10] D. A. Garanin, Phys. Rev. B **55**, 3050 (1997).
[11] D. A. Garanin and O. Chubykalo-Fesenko, Phys. Rev. B **70**, 212409 (2004).
[12] H. Suhl, IEEE Trans. Magn. **34**, 1834 (1998).
[13] V. L. Safonov and H. N. Bertram, Phys. Rev. B **63**, 094419 (2001).
[14] V. L. Safonov, J. Appl. Phys. **95**, 7145 (2004).
[15] H. Suhl, J. Phys. Chem. Solids **1**, 209 (1957).
[16] A. Yu. Dobin and R. H. Victora, Phys. Rev. Lett. **90**, 167203 (2003).
[17] P. Hasenfratz and F. Niedermayer, Z. Phys. B Condens. Matter **92**, 91 (1993).
[18] H. Kachkachi and D. A. Garanin, Eur. Phys. J. B **22**, 291 (2001).
[19] A. Kashuba, Phys. Rev. Lett. **96**, 047601 (2006).
[20] C. H. Back, R. Allenspach, W. Weber, S. S. P. Parkin, D. Weller, E. L. Garwin, and H. C. Siegmann, Science **285**, 864 (1999).
[21] B. Özyilmaz, A. D. Kent, D. Monsma, J. Z. Sun, M. J. Rooks, and R. H. Koch, Phys. Rev. Lett. **91**, 067203 (2003).
[22] D. A. Garanin, H. Kachkachi, and L. Reynaud, Europhys. Lett. **82**, 17007 (2008).
[23] R. Harris, M. Plischke, and M. J. Zuckermann, Phys. Rev. Lett. **31**, 160 (1973).
[24] E. M. Chudnovsky, in *The Magnetism of Amorphous Metals and Alloys*, edited by J. A. Fernandez-Baca and W.-Y. Ching (Word Scientific, Singapore, 1995).
[25] D. A. Garanin, Phys. Rev. B **53**, 11593 (1996).
[26] D. A. Garanin, Phys. Rev. B **75**, 094409 (2007).
[27] D. A. Garanin, Phys. Rev. B **77**, 024429 (2008).
[28] E. M. Chudnovsky and D. A. Garanin, Phys. Rev. Lett. **93**, 257205 (2004).